Acta Crystallographica Section D
Biological Crystallography
ISSN 0907-4449

Structure of the periplasmic copper-binding protein CueP from *Salmonella enterica* serovar Typhimurium

Bo-Young Yoon,[a] Yong-Hak Kim,[b] Nahee Kim,[c] Bo-Young Yun,[a] Jin-Sik Kim,[a] Joon-Hee Lee,[a] Hyun-Soo Cho,[b] Kangseok Lee[d] and Nam-Chul Ha[a]*

[a]College of Pharmacy, Pusan National University, Busan, Republic of Korea, [b]Department of Microbiology, School of Medicine, Catholic University of Daegu, Daegu, Republic of Korea, [c]Department of Biology, College of Science, Yonsei University, Seoul, Republic of Korea, and [d]Department of Life Science, Chung-Ang University, Seoul, Republic of Korea

Correspondence e-mail: hnc@pusan.ac.kr

Received 11 December 2012
Accepted 3 June 2013

PDB Reference: CueP, 4gqz

CueP was initially identified as a copper-resistance gene in *Salmonella enterica* serovar Typhimurium, which has evolved to survive in the phagosomes of macrophages. Recently, CueP was determined to be a periplasmic copper-binding protein and has been implicated in the transfer of copper ions to SodCII in the periplasm. In this study, the crystal structure of CueP has been determined, revealing a V-shaped dimeric structure. The conserved cysteine and histidine residues are clustered on the surface of one side of the C-terminal domain, suggesting that this cysteine- and histidine-rich region is related to the function of CueP. LC-MS/MS analysis established the presence of a disulfide bond between Cys96 and Cys176 under aerobic conditions. Subsequent biophysical analyses showed that the CueP protein binds copper and zinc, and the mutation of Cys104 to serine (C104S) dramatically reduced the binding affinity for copper and zinc, suggesting that the cysteine- and histidine-rich cluster is responsible for copper binding. This study provides a structural basis for the participation of CueP in the resistance of the intracellular pathogen *Salmonella* to copper.

1. Introduction

Salmonella enterica is a rod-shaped Gram-negative bacterium and is found in animals, including humans. In animals, *Salmonella* gastroenteritis caused by *S. enterica* leads to substantial morbidity, mortality and a considerable burden of disease globally (Coburn *et al.*, 2007). *Salmonella* can survive in macrophage phagosomes, an ability that is related to the virulence of the bacterium during systemic disease (Fields *et al.*, 1986).

The transition metal copper is essential for every living cell and functions as a key metal ion in electron-transporting proteins because of the easy conversion between Cu^{+} and Cu^{2+} (Nelson, 1999). However, Cu^{+} can generate highly toxic superoxide or hydroxyl radicals by reacting with molecular oxygen or hydrogen peroxide (Macomber *et al.*, 2007). In Gram-negative bacteria, excessive copper is primarily controlled by the *cue* regulon, which includes a sensor/transcriptional regulator protein CueR (Outten *et al.*, 2000). When Cu^{+} is detected by CueR in the cytoplasm, a P1B1-type ATPase CopA and the multicopper oxidase CueO are expressed (Rensing *et al.*, 2000; Outten *et al.*, 2000). CopA exports the cytoplasmic Cu^{+} into the periplasmic space, and CueO, which is located in the periplasm, rapidly catalyzes the conversion of Cu^{+} into the less toxic Cu^{2+} under aerobic conditions to prevent the toxic effects of Cu^{+} (Rensing *et al.*, 2000; Grass & Rensing, 2001).

In *Escherichia coli*, CueO is inactive under anaerobic conditions; copper resistance under such conditions thus

depends on the copper-ion exporter system CusABFC, which has a lower efficiency than CueO (Outten *et al.*, 2001). Cu^{+} is expelled into the external medium by the exporter CusABFC, which spans the inner membrane, the outer membrane and the periplasm (Franke *et al.*, 2003; Outten *et al.*, 2001; Long *et al.*, 2010; Xu *et al.*, 2009; Su *et al.*, 2009). Unlike CueO and CopA, expression of CusABFC is transcriptionally controlled by the two-component system CusR/CusS (Munson *et al.*, 2000).

CueP has recently been identified as a copper-resistance gene in *S. enterica* serovar Typhimurium (referred to as *S.* Typhimurium in this study) and functions as a substitute for the Cu^{+} exporter CusABFC (Pontel & Soncini, 2009). A *cueP*-deleted strain of *S.* Typhimurium was highly susceptible to copper, particularly under anaerobic conditions (Pontel & Soncini, 2009). CueP is induced by CueR (Pontel & Soncini, 2009), unlike CusABFC, and is only found in a subset of bacteria, whereas CusABFC is found in most Gram-negative bacteria. Gram-negative bacteria harbour either the CueR-regulated *cueP* locus or the CusRS-regulated *cus* locus (Pontel & Soncini, 2009). *S.* Typhimurium does not possess CusABFC but does possess CueP, even though *S.* Typhimurium is closely related to *E. coli*. Pontel and Soncini observed that the cysteine residues of CueP are specifically oxidized by Cu^{2+} and not by Fe^{3+} or Zn^{2+} (Pontel & Soncini, 2009). Osman and coworkers reported that CueP is a major copper-storage protein in the periplasm (Osman *et al.*, 2010). Very recently, CueP has also been characterized as an essential factor in the transfer of Cu^{2+} ions to the periplasmic SodCII protein to suppress oxidative stress (Osman *et al.*, 2013). However, the biochemical roles of CueP still remain largely unknown. In this study, we determined the crystal structure of CueP from *S.* Typhimurium at a resolution of 1.8 Å and this structure provided insight into the molecular mechanism of action of CueP.

2. Materials and methods

2.1. Cloning and expression

The DNA cloning, expression and purification of *S.* Typhimurium CueP (residues 22–179 based on the numbering of the precursor CueP) has been described previously (Yun *et al.*, 2011). The C104S mutation was introduced into the cloned wild-type *cueP* gene by two successive PCR reactions (Landt *et al.*, 1990) using the primers AGCCTTTCCGGCAGCCAGGGAGAAATG, CATTTCTCCCTGGCTGCCGGAAAGGCT, GGGCCATGGCATCCTCAGAATCCGCTTTT and GGGCTCGAGTTAACGTAATGGTAATTCCG.

2.2. Crystallization and data collection

The initial crystallization of CueP and the preliminary crystallographic analysis of a 2.5 Å resolution data set have been reported previously (Yun *et al.*, 2011). To determine the initial phases using the multiple-wavelength anomalous dispersion (MAD) method, selenomethionine-labelled CueP was crystallized. Crystals with a rod shape were obtained at 287 K in one month using the hanging-drop vapour-diffusion method. Equal volumes (1 µl) of 10 mg ml^{-1} protein solution and a reservoir solution consisting of 0.1 *M* sodium acetate pH 4.6, 2.0 *M* sodium chloride were mixed together. For cryoprotection, the crystals were briefly soaked in a solution consisting of 0.08 *M* sodium acetate pH 4.6, 1.6 *M* sodium chloride, 25%(*v*/*v*) glycerol. X-ray diffraction data were collected from flash-cooled crystals on BL44 at SPring-8, Hyogo, Japan at 100 K. Typical data sets consisted of 360 frames with 1° rotation and 1 s exposure time per image collected at wavelengths of 0.9790, 0.9792 and 0.9900 Å. The diffraction data sets were processed and scaled with the *HKL*-2000 package (Otwinowski & Minor, 1997).

2.3. Structural determination and refinement

The initial phases were obtained by the MAD method using the data set obtained from the selenomethionine-labelled CueP crystal described above. Eight selenium sites were found and were used for phase calculation in *SOLVE*; density modification and initial model building were subsequently performed using *RESOLVE* (Terwilliger & Berendzen, 1999). Model building was performed using *Coot* (Emsley & Cowtan, 2004) and model refinement was performed using the *PHENIX* package (Adams *et al.*, 2002). To refine the model, the data set collected at the peak wavelength (0.9790 Å) was used. A random set of 5% of the reflections was excluded from the refinement for cross-validation of the refinement strategy. Water molecules were assigned automatically for peaks of $>2\sigma$ in the $F_o - F_c$ difference maps by cycles of refinement using *PHENIX* (Adams *et al.*, 2002), and some of them were deleted by manual inspection. The quality of the model was checked using *MolProbity* (Chen *et al.*, 2010). All residues were in the favoured region of the Ramachandran plot. Detailed statistics for the X-ray data collection and refinement are presented in Table 1. The coordinates and structure factors have been deposited in the Protein Data Bank (PDB entry 4gqz). The figures were generated using *PyMOL* (DeLano, 2002).

2.4. Size-exclusion chromatography

To determine the molecular size of CueP and to confirm that it is a dimer in solution, size-exclusion chromatography was performed at a flow rate of 0.5 ml min^{-1} using a Superdex 200 HR 10/30 column (GE Healthcare) equilibrated with 20 m*M* Tris buffer pH 8.0 containing 150 m*M* NaCl and 2 m*M* β-mercaptoethanol.

2.5. Inductively coupled plasma mass spectrometry (ICP-MS)

The protein fractions (wild type or C104S mutant) eluted from the Ni–NTA resin were immediately desalted using a desalting column pre-equilibrated with 20 m*M* Tris buffer containing 50 m*M* NaCl and 2 m*M* β-mercaptoethanol without cleaving the hexahistidine tag. The protein sample (10 mg) was concentrated to 580 µ*M* (10 mg ml^{-1}) using an ultrafiltration device. The filtrate solution from the ultrafiltration was collected for use as a control. Each sample was subjected to ICP-MS to analyze for the presence of copper, zinc, calcium and nickel. An XSERIES 2 (Thermo, USA) was

Table 1
X-ray data-collection and refinement statistics.

Values in parentheses are for the highest resolution shell.

	SeMet		
Data set	Peak	Edge	Remote
Data collection			
Wavelength (Å)	0.9790	0.9792	0.9900
Resolution limits (Å)	50–1.80 (1.83–1.80)		
Space group	$P2_12_12_1$		
Unit-cell parameters (Å)	a = 58.5, b = 102.2, c = 114.2		
No. of unique reflections	118249	118879	117389
Multiplicity	5.1 (2.3)	5.0 (2.2)	4.9 (2.1)
$R_{\rm merge}$† (%)	10.2 (30.6)	9.8 (32.1)	12.0 (34.0)
Completeness (%)	97.5 (81.1)	97.0 (76.5)	96.3 (74.4)
Average $I/\sigma(I)$	26.5 (2.5)	26.3 (2.2)	25.7 (2.1)
Refinement			
R factor (%)	22.8		
$R_{\rm free}$‡ (%)	27.6		
Average B value (Å^2)	21.9		
Total No. of atoms	5412		
No. of water molecules	484		
R.m.s.d., bond lengths (Å)	0.008		
R.m.s.d., angles (°)	1.125		
Ramachandran plot (%)			
Most favoured	89.0		
Additionally allowed	11.0		
Generously allowed	0		
Disallowed	0		
PDB code	4gqz		

† $R_{\rm merge} = \sum_{hkl}\sum_i |I_i(hkl) - \langle I(hkl)\rangle| / \sum_{hkl}\sum_i I_i(hkl)$. ‡ $R_{\rm free}$ was calculated using 5% of the data set.

used for this study. The hexahistidine-tag-free CueP protein sample, which was also used for crystallization, was extensively dialyzed against 20 m*M* HEPES buffer pH 7.0 containing 2 m*M* β-mercaptoethanol. After concentration, the dialyzed protein sample (580 µ*M*) was also analyzed by ICP-MS as described.

2.6. Mass spectrometry

To examine modifications of cysteine and histidine residues in CueP, the purified hexahistidine-tag-free protein was dialyzed against 20 m*M* Tris–HCl pH 8.0, 150 m*M* NaCl and stored at 277 K for two weeks under aerobic conditions. The protein was then treated with 100 m*M* *N*-ethylmaleimide (NEM) and 6 *M* urea for 1 h to block the free thiol groups of cysteine residues and was subjected to acidic cleavage of the metal–thiolate complex during precipitation with 2 *M* trichloroacetic acid for 15 min on ice. After centrifugation, the precipitated protein was washed twice with pre-chilled 80% acetone. The air-dried protein was dissolved in 50 m*M* Tris–HCl pH 8.0 containing 6 *M* urea and 100 m*M* iodoacetamide (IAA) to block metal-complexing cysteine thiolates for 1 h in darkness. As experimental controls, the CueP protein was treated with 10 m*M* dithiothreitol (DTT) to reduce disulfide bonds for 15 min at room temperature prior to treatment with NEM or IAA. The protein was precipitated by treatment with 2 *M* trichloroacetic acid and 80% acetone. The air-dried protein was subsequently digested with sequencing-grade trypsin (Promega, Madison, Wisconsin, USA) and chymotrypsin (Roche Diagnostics GmbH, Mannheim, Germany) according to the manufacturer's manuals. The peptide clean-up, after acidification with 0.2% trifluoroacetic acid, was performed with ZipTip C18 (Millipore, Billerica, Massachusetts, USA) and the solvent was evaporated using a SpeedVac vacuum concentrator (Thermo Scientific, Asheville, North Carolina, USA). The dried peptides were dissolved in 0.4% acetic acid and analyzed on an LTQ-Velos mass spectrometer (Thermo Fisher Scientific Inc.) equipped with an EASY-nLC 1000 Liquid Chromatograph and a capillary column (75 µm inner diameter, 360 µm outer diameter, 7.5 cm length) packed with Magic C18AQ particles (5 µm, 200 Å pore size; Michrom Bioresources Inc., Auburn, California, USA). The chromatographic conditions were a 90 min linear gradient from 5 to 40% acetonitrile (ACN) in 0.1% formic acid (FA) followed by a 5 min column wash with 80% ACN/0.1% FA and a 25 min column re-equilibration step with 5% ACN/0.1% FA at a flow rate of 0.30 µl min^{-1}. Full mass scanning (MS) was performed between m/z 300 and 2000 and was followed by five data-dependent MS/MS scans with the following options: isolation width, $\pm 1.5 m/z$; normalized collision energy, 25%; dynamic exclusion duration, 30 s. The tandem mass-spectrometric data were analyzed using the *SEQUEST* search algorithm (Eng *et al.*, 1995) with the following options: average mass (m/z); precursor mass tolerance, 1.5 Da; fragment mass tolerance, 0.8 Da; variable modifications of cysteine by alkylation with NEM (m/z +125.13) or IAA (+57.02), oxidation (+15.99) and dioxidation (+31.99); histidine protonation (+1.01). The extracted ion chromatograms (XICs) were manipulated with Thermo *Xcalibur Qual Browser* v.2.1. Mass-spectrometric data for disulfide-bonded peptides were analyzed using an in-house *Excel* program with the option of 2H loss (−2.02) from all combinations of two peptides each containing a cysteine.

2.7. Measurement of the redox state of CueP

The sample-preparation method and reaction conditions were as described previously (Hiniker *et al.*, 2005) with minor modifications. The purified CueP protein was reduced for 10 min on ice with 10 m*M* DTT, and the DTT was then removed by buffer exchange into 20 m*M* Tris pH 8.0 buffer containing 150 m*M* NaCl using a desalting column (HiPrep 26/10; GE Healthcare). To measure the free thiol content of the protein sample (200 µl, 10 µ*M*), 10 µl of the incubated sample was added to 75 µl 30 m*M* Tris buffer pH 8.2 containing 3 m*M* EDTA. Subsequently, 5 m*M* DTNB and 99%(*v*/*v*) methanol were added and the mixture was incubated for 15 min at room temperature. After the reaction mixture had been centrifuged at 11 000*g* for 5 min, the amount of 2-nitro-5-thiobenzoate produced from disulfide-bond cleavage of DTNB by the thiol group of cysteine was quantified by measuring the absorption at 412 nm (ε = 14 150 M^{-1} cm^{-1}; Ellman, 1959).

3. Results and discussion

3.1. Structural determination

S. Typhimurium CueP was crystallized and its initial phases were determined by the multiple-wavelength anomalous

diffraction approach using selenomethionine-incorporated crystals. A high-quality electron-density map was produced and the majority of the model could be traced. The crystals contained four protomers in the asymmetric unit. The final model of CueP was refined to 1.8 Å resolution. All 158 residues were present in the model, with the exception of residues 50–52 in two of the four protomers. The structure was refined to a free R value of 26.4% with good stereochemistry. Further details of the structure determination and refinement are given in Table 1.

3.2. Overall structure

The four CueP molecules in the asymmetric unit were related by two orthogonal noncrystallographic twofold axes, forming a dimer of dimers as shown in Fig. 1(*a*). Each protomer consists of two domains: the N-terminal domain and C-terminal domain (residues 22–79 and 80–179, respectively). The overall fold of CueP is shown in Figs. 1(*b*) and 1(*c*). The N-terminal domain has a mixed α/β-type fold consisting of two α-helices and three β-strands that are organized into a β-sheet. The larger C-terminal domain comprises a four-stranded β-sheet and a two-stranded β-sheet that face each other. No significant movement between the domains was observed when the four protomers were superimposed (Fig. 1*d*). The four molecules in the asymmetric unit are almost identical, with overall root-mean-square deviations calculated for the C^{α} atoms between the four protomers ranging from 0.12 to 0.36 Å (Fig. 1*d*). The two neighbouring molecules make extensive contacts, forming an overall V-shape (burying 2200 Å^2 of the surface area of 7300 Å^2). The N-terminal domain is solely involved in the dimer interaction (Fig. 1*a*); the C-terminal

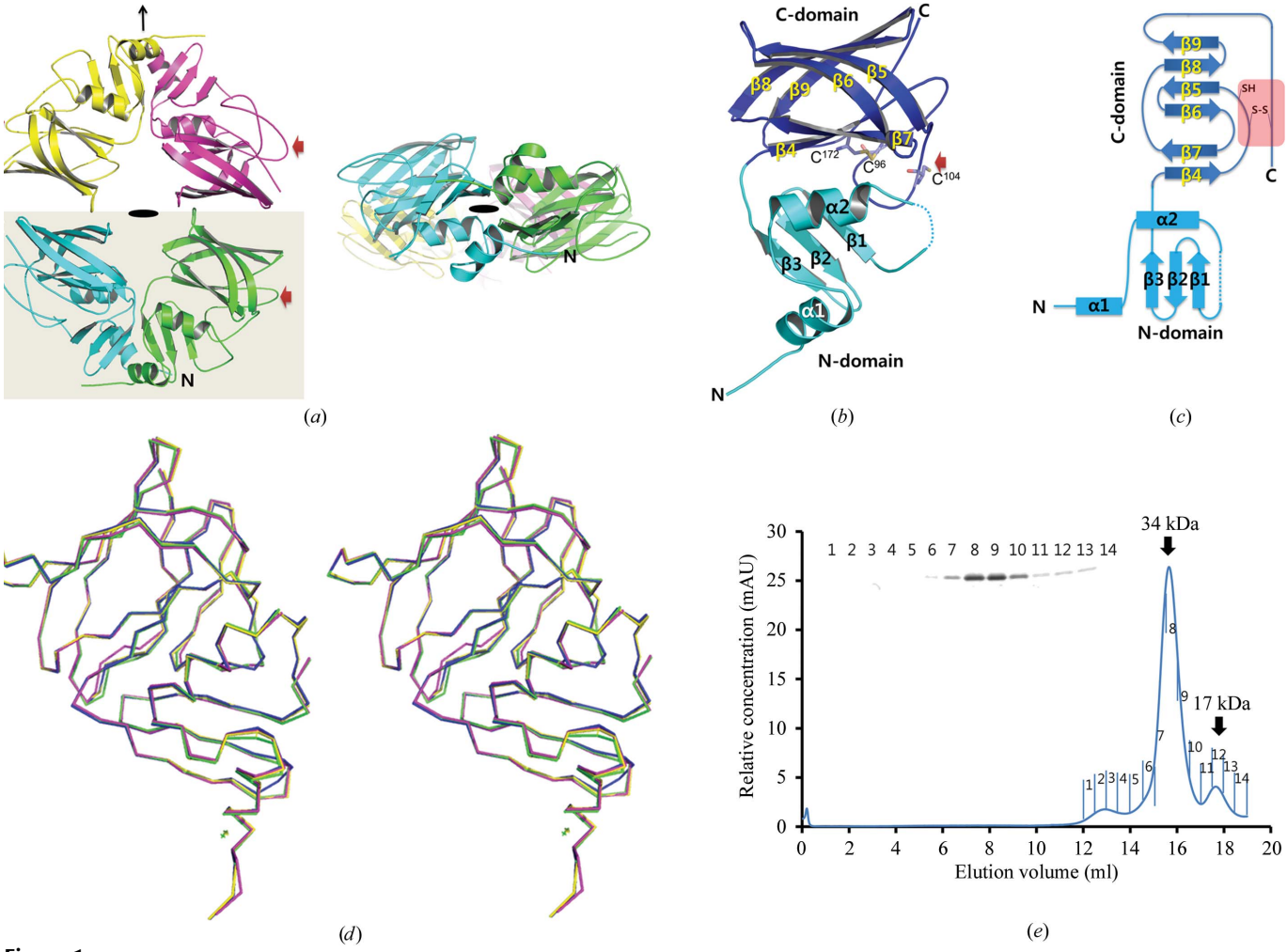

Figure 1
Overall structure of *S.* Typhimurium CueP. (*a*) Ribbon representation of the asymmetric unit of CueP. Each protomer is drawn in a different colour. The two dimeric units are arranged based on the twofold rotational axis. The dimeric units displaying a V-shape are shown with a grey background. The red arrows indicate the key conserved region. (*b*) Ribbon representation of the CueP protomer. The N-terminal and C-terminal domains are displayed in cyan and blue, respectively. The disulfide bond is shown in yellow. Each secondary-structural element is numbered. (*c*) Schematic drawing of the folding topology of the CueP protomer. The colour profile and the secondary-structural element numbering are the same as in (*b*). (*d*) Stereoview of the structural superposition of the four protomers in the asymmetric unit. Each protomer is displayed as a C^{α} representation and is coloured differently (magenta, green, blue and yellow). (*e*) Elution profile from a size-exclusion chromatography column (Superdex 200 10/30). The calculated molecular weights are shown above each peak. Each fraction was analyzed by SDS–PAGE.

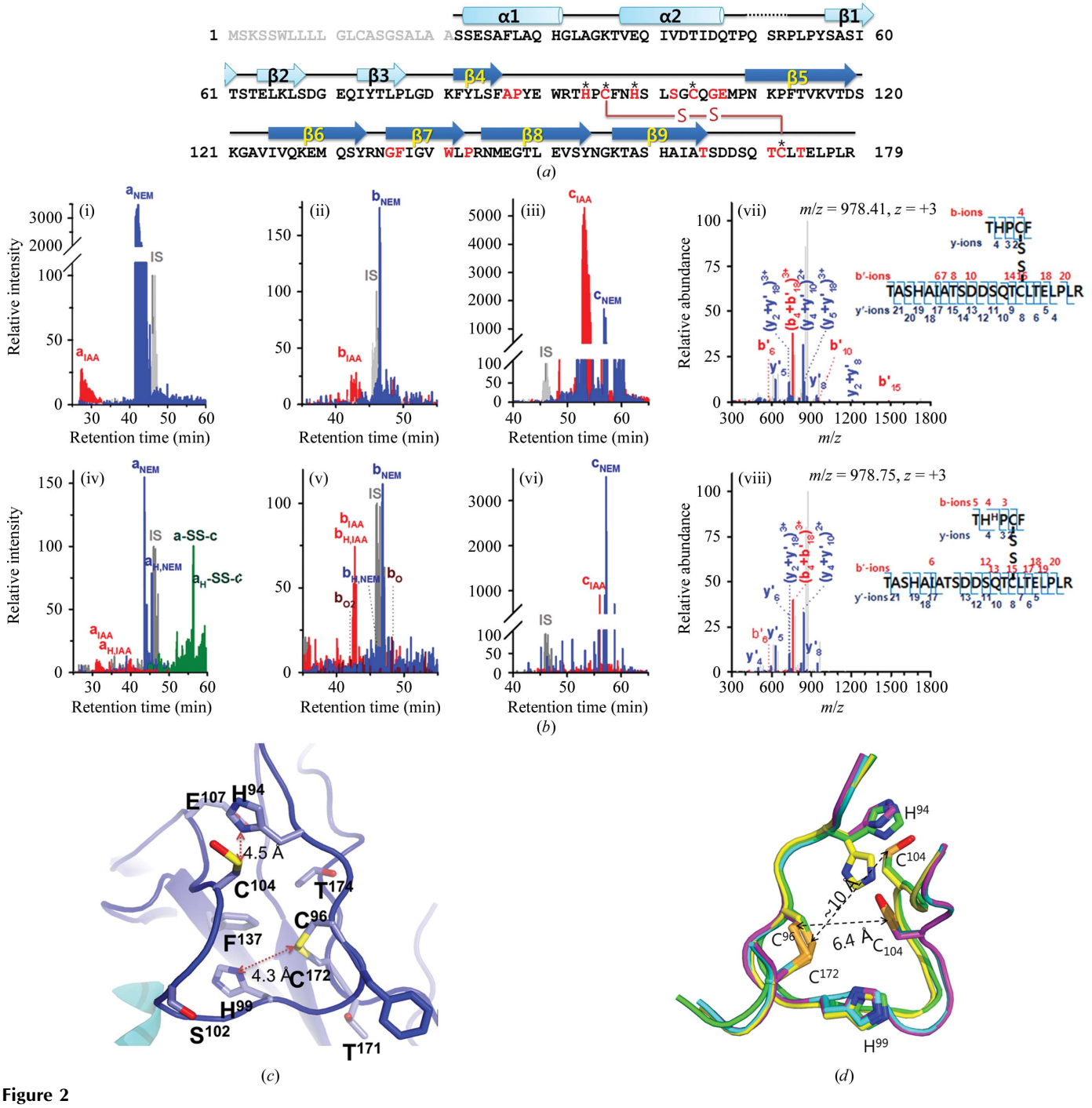

Figure 2

The putative active site of CueP in the crystal structure. (*a*) Amino-acid sequence of *S.* Typhimurium CueP together with the secondary-structure elements. The key conserved residues are shown in red. The disulfide bridge which was observed in the crystal structure is shown as a red line labelled 'S–S'. The signal sequence is shown in grey. (*b*) Extracted ion chromatograms (XICs) of the three cysteine-containing peptides in CueP prepared (i–iii) under reducing conditions for determination of reference peaks of the peptides derivatized with NEM or IAA at the same protein concentrations and (iv–vi) under nonreducing conditions for examination of variable modifications of cysteine and histidine residues. The XIC peak letters, a, b and c, represent the precursor ions of ^{93}THPCF^{97}, ^{98}NHSLSGCQGEMPNKPF^{113} and ^{162}TASHAIATSDDSQTCLTELPLR^{183}, respectively, and variable modifications are denoted after the peak letters with the following subscripts: NEM or IAA, alkylation of cysteine with *N*-ethylmaleimide or iodoacetamide; O or O2, mono- or di-oxidation of cysteine; H, protonation of His94 or His99. The relative intensity of XIC was calculated in relation to the peak intensity of an unmodified peptide, LSDGEQIY (m/z = 462.99, z = +2 at RT, 46.0 min), which was used as an internal standard (IS) and expressed as 100. Tandem mass spectra of the precursor ions of disulfide-bonded (–SS–) peptides are assigned to the b and y ions generated from collision-induced fragmentation of ^{93}THPCF^{97} and ^{162}TASHAIATSDDSQTCLTELPLR^{183} with a cross-link between Cys96 and Cys172 and unprotonated (vii) (m/z = 978.41, z = +3) or protonated (viii) (m/z = 978.75, z = +3) His94 (H^H). Other tandem mass spectra with variable modifications at cysteine and histidine residues are shown in Supplementary Fig. S2. (*c*) Structure of the key conserved region. The conserved Cys96 and Cys172 residues form the disulfide bridge and Cys104 exists as a sulfenic acid in the crystal structure. The highly conserved residues His94, His99, Thr171, Thr174 and Glu107 are also displayed. (*d*) Structural superposition of the putative active sites of the four protomers in the asymmetric unit. Each protomer is coloured differently. The side chains of His94, Cys96, His99, Cys104 and Cys172 are shown.

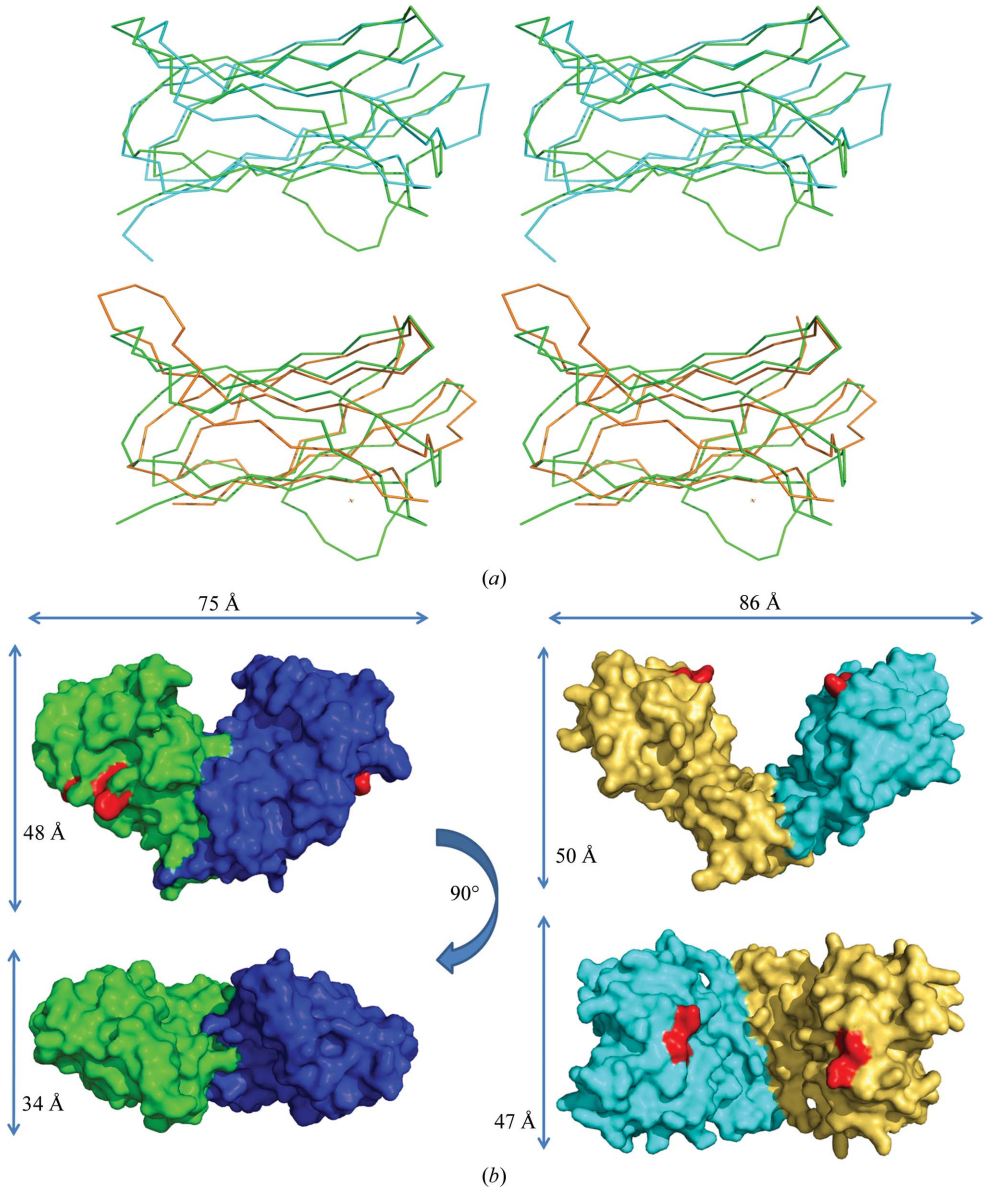

Figure 3
Structural comparison of CueP. (*a*) Stereo figures showing C^{α} superpositions of the CueP C-terminal domain (80–179) with transglutaminase (PDB entry 3e8v; residues 289–366) and pyrogallol hydroxytransferase (PDB entry 1ti6; residues 194–294). CueP is displayed in green, transglutaminase in orange and pyrogallol hydroxytransferase in cyan. (*b*) Surface representation of CueP (left) and *E. coli* DsbC (right; PDB entry 1eej; McCarthy *et al.*, 2000) in two different orientations (top and bottom). Each protomer is coloured differently (green and blue for CueP; yellow and cyan for DsbC). The cysteine-rich (putative) active sites are coloured red.

domains of the dimeric unit form the two wings of the V-shaped structure. However, there is only slight contact between the two V-shaped dimers in the asymmetric unit, indicating that this interaction does not represent a physiological interaction (Fig. 1*a*).

We next used size-exclusion chromatography to examine whether the V-shaped dimeric unit of CueP represents the structure in solution. The main peak corresponded to the dimeric form of CueP (Fig. 1*e*). Thus, it is likely that the dimeric structure that is observed in the crystal is preserved in solution.

3.3. Putative active site

Sequence alignment of CueP homologue proteins revealed that most of the conserved residues are clustered in two adjacent loops (the $\beta4$–$\beta5$ loop and the C-terminal loop; Fig. 2*a*). The crystal structure of CueP revealed that a disulfide bridge is formed by the strictly conserved residues Cys96 and Cys172 in the two loops and these disulfide bonds are located in the outer wing region in the V-shaped dimeric structure. Cys96 is exposed to the solvent, whereas Cys172 is relatively buried in the structure. This disulfide pair appears to be generated by oxidation by molecular oxygen. Ellman's assay revealed that the protein sample was gradually oxidized as the protein sample was stored at 277 K in the absence of a reducing agent (Supplementary Fig. S1[1]).

Mass-spectrometric analysis proved that CueP forms a disulfide bond between the Cys96 and Cys172 residues under nonreducing conditions (Fig. 2*b*). In addition, the Cys104 residue was subjected to a certain amount of oxidation to produce cysteine sulfenic acid (–SOH) and sulfinic acid ($-SO_2H$). Consistent with this result, electron density was found protruding from Cys104 S^{γ} in the crystal structure, which could be interpreted as cysteine sulfenic acid (Supplementary Fig. S3). No metal ion was found in this cysteine-rich region of CueP, suggesting that the oxidized CueP is not in a chemical state capable of coordinating a metal ion.

In order to analyze the metal-complexing cysteine thiolate in CueP in the reduced state by mass spectrometry, the free thiol group of the cysteine of freshly prepared CueP was alkylated with NEM prior to acidic cleavage of the metal–thiolate complex by treatment with 2 *M* trichloroacetic acid and was then subjected to differential alkylation with IAA. Extracted ion chromatograms showed a relatively high level of

[1] Supplementary material has been deposited in the IUCr electronic archive (Reference: CB5028). Services for accessing this material are described at the back of the journal.

Cys104 modified by IAA compared with Cys96 and Cys192, which indicated that Cys104 has a high potential to form a metal–thiolate complex.

To support this finding, two conserved histidine residues (His94 and His99) are present in the $\beta4$–$\beta5$ loop and are located close to Cys172 and Cys104, respectively (Fig. 2*c*). The interatomic distances between the N^{ε} atom of the imidazole group and the S atom in the His94–Cys104 and His99–Cys172 pairs are 4.5 and 4.3 Å, respectively. Although the position of the imidazole group of the buried His99 is fixed, that of the exposed His94 is highly flexible (Fig. 2*d*). The loop containing Cys104 seems to be intrinsically flexible because the loops from two protomers are significantly different from the loops from the other protomers. Because these cysteine and histidine residues are strictly conserved among all CueP homologues, it is highly probable that this cysteine- and histidine-rich region plays an important role in the metal ion-binding function of CueP. Thus, we designated this region as a putative active site.

3.4. Structural comparison with other proteins

To find proteins with a similar fold, we used the individual domains of CueP in a search with the *DALI* server (Holm & Rosenström, 2010). The *DALI* server only gave low-quality models for the N-terminal domain (residues 22–79) of CueP. However, the models returned by the *DALI* server for the C-terminal domain (80–179) were of better quality. A transglutaminase family protein (PDB entry 3e8v; r.m.s.d. 2.0 Å and *Z*-score of 8.5 between 78 residues; New York SGX Research Center for Structural Genomics, unpublished work) and the pyrogallol hydroxytransferase large subunit (PDB entry 1ti6; r.m.s.d. 2.0 Å and *Z*-score of 8.5 between 80 residues; Messerschmidt *et al.*, 2004) were found. As shown in Fig. 3, the overall folds of the proteins are very similar. However, the cysteine residues at the putative active site were not found in these proteins. Hence, these proteins with similar folds do not appear to have a functional relationship to CueP.

3.5. Copper binding of CueP

A previous report suggested that CueP is a copper-storage protein (Osman *et al.*, 2010). Because cysteine and histidine residues can coordinate metal ions, the cysteine- and histidine-rich region might be involved in metal coordination in the reduced state. The specific oxidation of CueP by copper ions which was observed in a previous study (Pontel & Soncini, 2009) also suggests the presence of a copper-binding site in CueP. To determine which metal ions bind to CueP, we performed inductively coupled plasma mass spectrometry (ICP-MS) experiments with the purified CueP protein. The protein sample was eluted from Ni–NTA resin and then promptly desalted to remove the trace amount of unbound metal ions. The CueP sample was subjected to ICP-MS under reducing conditions after concentration by ultrafiltration. To exclude the influence of the metals in the buffer solution, the metal content of the filtrate solution from the ultrafiltration step was also analyzed (Table 2). The result showed that significant amounts of copper were bound to the CueP protein, which is consistent with previous results (Osman *et al.*, 2010, 2013). Interestingly, as much zinc as copper was bound to the CueP protein. However, it seemed that calcium was not specifically bound to CueP because calcium was also observed in the filtrate solution. Nickel was enriched in the protein sample, possibly as a result of the hexahistidine tag in the protein.

To remove weakly and nonspecifically bound ions from the protein, the hexahistidine tag was removed from the protein sample and the protein was further purified by size-exclusion chromatography followed by extensive dialysis against a metal-free buffer. The ICP-MS results revealed that the protein retained copper and zinc, whereas calcium and nickel were substantially removed (Table 2). These observations suggest that the metal-binding site(s) of CueP are specific for copper and/or zinc and that the binding affinities for these metals are relatively strong.

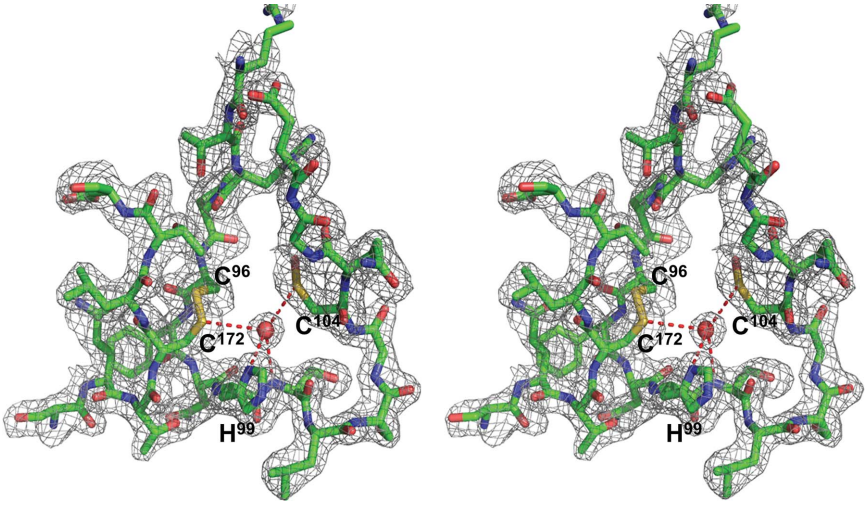

Figure 4
Stereo figure of the electron-density map surrounding the water molecule bound in the putative active site. The $2F_o - F_c$ map contoured at 1.0σ is drawn in grey and the bound water molecule is represented by a red sphere. Hydrogen bonds are represented by red dotted lines.

3.6. A candidate site for copper binding

A water molecule was strongly bound to the putative active site in the crystal structure, which represents an oxidized state. The water molecule was trapped by interactions with Cys96, Cys172, His99 and a backbone NH group (Fig. 4). Cys104 is also close enough to interact with the water molecule. The three conserved cysteine residues in the purified CueP protein could partly coordinate with metal ions in the reduced state and this structure provides clues about the structure of the copper binding state. If Cys96 and Cys172 are reduced and if rotation of the Cys104 S^{γ} atom is allowed, Cu^{+}

Table 2
Metal:CueP ratios determined by ICP-MS.

Each sample contained the protein at 580 μ*M*. The hexahistidine-tagged proteins (wild-type His-CueP and C104S His-CueP) were not subjected to dialysis to remove free metals. However, the intact CueP protein (wild-type $CueP_{dialysis}$) was extensively dialyzed against a metal-free buffer. The detection limit of each metal was less than 0.000003. ND, not detected.

	Wild-type His-CueP (filtrate)	Wild-type $CueP_{dialysis}$ (filtrate)	C104S His-CueP (filtrate)
Copper	0.2 (0.001)	0.1 (ND)	0.008 (ND)
Zinc	0.4 (ND)	0.4 (ND)	0.05 (ND)
Calcium	0.03 (0.06)	0.003 (ND)	0.01 (ND)
Nickel	0.1 (ND)	0.004 (ND)	0.3 (ND)

or Cu^{2+} could be coordinated by Cys96, Cys172, Cys104 and His99 in place of the bound water molecule, replacing the unknown metal ion in the reduced state. Given the short distance, it is likely that His94 forms a hydrogen bond to the thiol group of Cys104, forming a thiolate anion, which facilitates coordination with a metal ion. Furthermore, the LC-MS/MS analysis indicated that Cys104 is involved in formation of the metal–thiolate complex (Fig. 2*b*). To determine whether this site participates in copper binding, we performed an ICP-MS experiment with a mutant CueP protein (C104S). The amounts of bound copper and zinc were drastically reduced (Table 2), indicating that the putative copper-binding site is responsible for copper and zinc ion binding, as expected from the structure. However, the binding of zinc ion might not be important for the role of CueP since zinc has not been functionally related to the protein.

During the review of this manuscript, Osman and coworkers reported that the function of CueP is associated with copper-ion transfer to the periplasmic superoxide dismutase (SodCII), preventing the damage caused by ROS (Osman *et al.*, 2013). They also reported that the copper content of the CueP protein was close to 1.0 Cu atoms per protein molecule when the protein was expressed in *E. coli* in medium supplemented with copper (Osman *et al.*, 2013). We speculate that this putative metal-binding site plays a central role in the copper-transfer process. To visualize the molecular features involved in copper binding, we attempted to determine the crystal structure of the protein in complex with copper. However, we were not able to obtain crystals, most likely owing to the strong intermolecular disulfide bonds induced by copper ions, as observed previously (Pontel & Soncini, 2009).

4. Conclusion

We determined the crystal structure of CueP from *S.* Typhimurium, which provides the first structural information about a CueP homologue. The crystal structure revealed that the strictly conserved cysteine and histidine residues are clustered at the putative active site, suggesting that this region may be responsible for the function of CueP. The mass-spectrometric and ICP-MS results indicate that CueP has a copper- and/or zinc-binding site at the putative active site. Although further investigation is required in order to understand the molecular mechanism by which CueP participates in the resistance of the intracellular pathogen *Salmonella* to copper, our findings suggest that the copper-binding ability of this protein might be necessary for the action of CueP.

This work was supported by a grant from the National Research Foundation of Korea (NRF-2012-0005548) to N-CH. This study made use of BL44 at SPring-8 (Japan), which was also supported by Pohang Accelerator Laboratory (Republic of Korea). The authors declare that there are no competing commercial interests related to this work.

References

Adams, P. D., Grosse-Kunstleve, R. W., Hung, L.-W., Ioerger, T. R., McCoy, A. J., Moriarty, N. W., Read, R. J., Sacchettini, J. C., Sauter, N. K. & Terwilliger, T. C. (2002). *Acta Cryst.* D**58**, 1948–1954.
Chen, V. B., Arendall, W. B., Headd, J. J., Keedy, D. A., Immormino, R. M., Kapral, G. J., Murray, L. W., Richardson, J. S. & Richardson, D. C. (2010). *Acta Cryst.* D**66**, 12–21.
Coburn, B., Grassl, G. A. & Finlay, B. B. (2007). *Immunol. Cell Biol.* **85**, 112–118.
DeLano, W. L. (2002). *PyMOL.* http://www.pymol.org.
Ellman, G. L. (1959). *Arch. Biochem. Biophys.* **82**, 70–77.
Emsley, P. & Cowtan, K. (2004). *Acta Cryst.* D**60**, 2126–2132.
Eng, J. K., McCormack, A. L. & Yates, J. R. III (1994). *J. Am. Soc. Mass. Spectrom.* **5**, 976–989.
Fields, P. I., Swanson, R. V., Haidaris, C. G. & Heffron, F. (1986). *Proc. Natl Acad. Sci. USA*, **83**, 5189–5193.
Franke, S., Grass, G., Rensing, C. & Nies, D. H. (2003). *J. Bacteriol.* **185**, 3804–3812.
Grass, G. & Rensing, C. (2001). *Biochem. Biophys. Res. Commun.* **286**, 902–908.
Hiniker, A., Collet, J.-F. & Bardwell, J. C. A. (2005). *J. Biol. Chem.* **280**, 33785–33791.
Holm, L. & Rosenström, P. (2010). *Nucleic Acids Res.* **38**, W545–W549.
Landt, O., Grunert, H.-P. & Hahn, U. (1990). *Gene*, **96**, 125–128.
Long, F., Su, C.-C., Zimmermann, M. T., Boyken, S. E., Rajashankar, K. R., Jernigan, R. L. & Yu, E. W. (2010). *Nature (London)*, **467**, 484–488.
Macomber, L., Rensing, C. & Imlay, J. A. (2007). *J. Bacteriol.* **189**, 1616–1626.
McCarthy, A. A., Haebel, P. W., Törrönen, A., Rybin, V., Baker, E. N. & Metcalf, P. (2000). *Nature Struct. Biol.* **7**, 196–199.
Messerschmidt, A., Niessen, H., Abt, D., Einsle, O., Schink, B. & Kroneck, P. M. H. (2004). *Proc. Natl Acad. Sci. USA*, **101**, 11571–11576.
Munson, G. P., Lam, D. L., Outten, F. W. & O'Halloran, T. V. (2000). *J. Bacteriol.* **182**, 5864–5871.
Nelson, N. (1999). *EMBO J.* **18**, 4361–4371.
Osman, D., Patterson, C. J., Bailey, K., Fisher, K., Robinson, N. J., Rigby, S. E. & Cavet, J. S. (2013). *Mol. Microbiol.* **87**, 466–477.
Osman, D., Waldron, K. J., Denton, H., Taylor, C. M., Grant, A. J., Mastroeni, P., Robinson, N. J. & Cavet, J. S. (2010). *J. Biol. Chem.* **285**, 25259–25268.
Otwinowski, Z. & Minor, W. (1997). *Methods Enzymol.* **276**, 307–326.
Outten, F. W., Huffman, D. L., Hale, J. A. & O'Halloran, T. V. (2001). *J. Biol. Chem.* **276**, 30670–30677.
Outten, F. W., Outten, C. E., Hale, J. & O'Halloran, T. V. (2000). *J. Biol. Chem.* **275**, 31024–31029.
Pontel, L. B. & Soncini, F. C. (2009). *Mol. Microbiol.* **73**, 212–225.
Rensing, C., Fan, B., Sharma, R., Mitra, B. & Rosen, B. P. (2000). *Proc. Natl Acad. Sci. USA*, **97**, 652–656.
Su, C.-C., Yang, F., Long, F., Reyon, D., Routh, M. D., Kuo, D. W., Mokhtari, A. K., Van Ornam, J. D., Rabe, K. L., Hoy, J. A., Lee,

Y. J., Rajashankar, K. R. & Yu, E. W. (2009). *J. Mol. Biol.* **393**, 342–355.
Terwilliger, T. C. & Berendzen, J. (1999). *Acta Cryst.* D**55**, 849–861.
Xu, Y., Yun, B.-Y., Sim, S.-H., Lee, K. & Ha, N.-C. (2009). *Acta Cryst.* F**65**, 743–745.
Yun, B.-Y., Piao, S., Kim, Y.-G., Moon, H. R., Choi, E. J., Kim, Y.-O., Nam, B.-H., Lee, S.-J. & Ha, N.-C. (2011). *Acta Cryst.* F**67**, 675–677.